



**A NON-ALIGNED DEEP TRANSLATION REPRESENTATION TO
APPROXIMATE VASCULAR NARROW BAND POLYP PATTERNS FROM
STANDARD COLONOSCOPY SEQUENCES.**

FRANKLIN SAMUEL SIERRA JEREZ

**UNIVERSIDAD INDUSTRIAL DE SANTANDER
FACULTAD DE INGENIERÍAS FÍSICOMEcÁNICAS
ESCUELA DE INGENIERÍA DE SISTEMAS E INFORMÁTICA
BUCARAMANGA**

2023

**A NON-ALIGNED DEEP TRANSLATION REPRESENTATION TO
APPROXIMATE VASCULAR NARROW BAND POLYP PATTERNS FROM
STANDARD COLONOSCOPY SEQUENCES.**

FRANKLIN SAMUEL SIERRA JEREZ

**Research work in partial fulfillment of the requirements for the degree of:
Magíster en Ingeniería de Sistemas e Informática**

Advisor:

Fabio Martínez Carrillo

Ph.D in Systems and Computer Engineering

**UNIVERSIDAD INDUSTRIAL DE SANTANDER
FACULTAD DE INGENIERÍAS FÍSICOMEcÁNICAS
ESCUELA DE INGENIERÍA DE SISTEMAS E INFORMÁTICA
BUCARAMANGA
2023**

ACKNOWLEDGEMENTS

To my parents, José Sierra and Zoraida Jerez, who gave me their support in my decision to apply, and overall for continuing in my master's program; for their advice and motivation any time that I needed it (which were not few). To my brother, Cristian Sierra, to encourage him to continue pursuing his dreams, and like me, someday find his horizon as an engineer in something that he truly loves. All of you are the infinite fuel that I was fortunate to be able to have in moments of weakness. All of you are the ones that drive me to keep going and to be better every day. At the Universidad Industrial de Santander, the Facultad de ingeniería fisicomecánicas, and the Escuela de Ingeniería de Sistemas e Informática; for allowing me to go beyond my initial dream of being a professional: the privilege of continuing my training as a researcher. To the *Bivl²ab* research group for giving me the opportunity to continue and grow in all my professional aspects, and allowing me to learn a little more about the rigorous but fascinating research world. To Professor Fabio Martínez Carrillo, for giving me the honor of continuing under his guidance, vocation, infinite patience, and professionalism. He is a real example of what the word professional means. Professor Fabio Martínez Carrillo thank you very much for your constant advice, and teachings, and for motivating me to continue preparing myself as a researcher.

I dedicate this book to my parents and my brother. This book, which I hope will be the first of many written in a foreign language, is yours.

CONTENTS

	page
INTRODUCTION	11
1. FUNDAMENTALS	14
1.1. Clinical polyp characterization	14
1.2. Computational approaches to characterize polyp malignancy	18
1.2.1 Classification methods	18
1.2.2 Generative mechanisms as biomarker descriptors	19
1.3. Related work	21
2. RESEARCH PROBLEM	24
2.1. Research question	25
3. OBJECTIVES	26
3.1. General objective	26
3.2. Specific objectives	26
4. PROPOSED APPROACH	27
4.1. Polyp vascular features mapping from NBI to OC	28
4.2. An embedding polyp-class representation	30
5. EXPERIMENTAL SETUP	32
5.1. Data	32
5.2. Model setup	34
6. EVALUATION AND RESULTS	36

7. DISCUSSION	46
8. CONCLUSIONS AND FUTURE WORK	49
BIBLIOGRAPHY	50
APPENDIX OF ACADEMIC PRODUCTS	55

LIST OF FIGURES

	page
Figure 1. Macroscopic and microscopic appearance for each type of polyp.	15
Figure 2. Macroscopic appearance for each type of polyp under OC and NBI light. . . .	17
Figure 3. Method for the classification of colorectal polyps.	18
Figure 4. Cyclegan network for non-aligned domain translation	20
Figure 5. General pipeline of the proposed approach	28
Figure 6. Ablation study for the polyp classification task on NBI sequences.	37
Figure 7. Qualitative results of the image translation from OC to NBI.	41
Figure 8. Boxplots of neoplastic probability across the three main types of polyps. . . .	42
Figure 9. Image traduction quality	43
Figure 10. Image traduction over owner dataset	45

LIST OF TABLES

	page
Table 1. Polyp classification performance over different colonoscopy sequences.	39
Table 2. Confusion matrix for adenoma-hyperplastic polyp classification.	40
Table 3. Image traduction quality over an aligned public dataset.	44

LIST OF APPENDICES

	page
Appendix A. Academic Products	55

ABSTRACT

TITLE: A NON-ALIGNED DEEP TRANSLATION REPRESENTATION TO APPROXIMATE VASCULAR NARROW BAND POLYP PATTERNS FROM STANDARD COLONOSCOPY SEQUENCES *

AUTHOR: FRANKLIN SAMUEL SIERRA JEREZ **

KEYWORDS: COLORECTAL CANCER, NARROW BAND IMAGING (NBI), OPTICAL COLONOSCOPY (OC), POLYP CHARACTERIZATION, NON-ALIGNED PROJECTIONS.

DESCRIPTION: Polyps are the main colorectal cancer biomarker, being their vascular patterns fundamental to categorizing disease malignancy. These patterns are typically observed *in situ* from specialized narrow-band images (NBI). Nonetheless, the categorization remains biased for expert observations, reporting errors in classification from 59.5% to 84.2%. Besides, a current challenge today is to achieve polyp malignancy categorization from standard colonoscopies. This work introduces a computational strategy that allows polyp malignancy classification from standard colonoscopies, recovering vascularity from a translation task. For doing so, a non-aligned translation task from optical colonoscopy (OC) to NBI, allows the deep representation adjustment. In a retrospective study, the enhanced optical sequences were validated with respect to discrimination capability among adenomas and hyperplastic samples achieving an F1 score of 0.86%. The study group included 8 adenoma videos (4524 frames) and 4 hyperplastic sequences (952 frames). Additionally, serrated samples were projected to the trained representation, achieving statistical differences from the adenomas and hyperplastic samples with a ρ -value < 0.05 according to the Mann-Whitney U test.

* Research work

** Facultad de ingenierías fisicomecánicas. Escuela de ingeniería de sistemas e informática. Advisor: Fabio Martínez Carrillo, Ph.D.

RESUMEN

TÍTULO: UNA REPRESENTACIÓN DE TRASLACIÓN PROFUNDA NO ALINEADA PARA APROXIMAR PATRONES VASCULARES DE PÓLIPOS DE BANDA CERCANA A PARTIR DE SECUENCIAS DE COLONOSCOPIA ESTÁNDAR *

AUTOR: FRANKLIN SAMUEL SIERRA JEREZ **

PALABRAS CLAVE: CÁNCER COLORECTAL, IMAGEN DE BANDA CERCANA (NBI), COLONOSCOPIA ÓPTICA (OC), CARACTERIZACIÓN DE PÓLIPOS, PROYECCIONES NO ALINEADAS.

DESCRIPCIÓN: Los pólipos son el principal biomarcador del cáncer colorrectal, siendo sus patrones vasculares fundamentales para categorizar la malignidad de la enfermedad. Estos patrones se observan típicamente *in situ* a partir de imágenes especializadas de banda estrecha (NBI, por sus siglas en inglés). No obstante, esta categorización sigue siendo sesgada incluso en las observaciones de expertos, reportando errores en la clasificación que van desde el 59.5% hasta el 84.2%. Un desafío actual es lograr la categorización de la malignidad de los pólipos a partir de colonoscopias estándar. Este trabajo presenta una estrategia computacional que permite la clasificación de la malignidad de los pólipos a partir de colonoscopias estándar, recuperando la vascularidad mediante una tarea de traducción. Para hacerlo, una tarea de traducción no alineada desde la colonoscopia óptica (OC) hasta NBI permite el ajuste de la representación profunda. En un estudio retrospectivo, las secuencias ópticas mejoradas se validaron en cuanto a su capacidad de discriminación entre adenomas y muestras hiperplásicas logrando una puntuación F1 del 0.86%. El grupo de estudio incluyó 8 videos de adenomas (4524 fotogramas) y 4 secuencias hiperplásicas (952 fotogramas). Además, las muestras serradas se proyectaron en la representación entrenada, logrando diferencias estadísticas con respecto a los biomarcadores de tipo adenoma e hiperplásicas con un valor de ρ -value < 0.05 según el test de U de Mann-Whitney.

* Trabajo de investigación

** Facultad de ingenierías fisicomecánicas. Escuela de ingeniería de sistemas e informática. Director: Fabio Martínez Carrillo, Ph.D.

INTRODUCTION

Colorectal cancer (CRC) was responsible in 2020 for about one million deaths, being the third most frequent cancer and the second most lethal cancer worldwide¹. Currently, CRC reports a mortality rate of 49.21% with an increasing projection of 60% in 2030². Polyps are the main CRC biomarkers mainly categorized according to shape, color, glandular texture, intestinal location, and microvascular patterns³. The gold standard for polyp classification is carried out from histological inspection, coarsely grouping: in hyperplastic (without clinical risk) being the 29–42% of CRC biomarkers and neoplastic adenoma that represents the rest of lesions⁴. Additionally, serrated samples have currently been proposed as a new category of polyps that share adenoma-hyperplastic patterns, which are precursors of at least 30% of CRC cases⁵. Despite that an early neoplastic polyps polypectomy increases the survival rate by 90%⁶, the characterization from standard colonoscopies remains challenging and expert dependent (kappa

-
- ¹ Leonardo Zorron Cheng Tao Pu et al. “Computer-aided diagnosis for characterization of colorectal lesions: comprehensive software that includes differentiation of serrated lesions”. In: *Gastrointestinal endoscopy* 92.4 (2020), pp. 891–899.
- ² Hyuna Sung et al. “Global cancer statistics 2020: GLOBOCAN estimates of incidence and mortality worldwide for 36 cancers in 185 countries”. In: *CA: a cancer journal for clinicians* 71.3 (2021), pp. 209–249.
- ³ Kangkana Bora et al. “Computational learning of features for automated colonic polyp classification”. In: *Scientific Reports* 11.1 (2021), pp. 1–16.
- ⁴ Juan Francisco Ortega-Morán et al. “Medical needs related to the endoscopic technology and colonoscopy for colorectal cancer diagnosis”. In: *BMC cancer* 21.1 (2021), pp. 1–12.
- ⁵ Ignasi Puig and Tonya Kaltenbach. “Optical diagnosis for colorectal polyps: a useful technique now or in the future?” In: *Gut and Liver* 12.4 (2018), p. 385.
- ⁶ Prashanth Rawla, Tagore Sunkara, and Adam Barsouk. “Epidemiology of colorectal cancer: incidence, mortality, survival, and risk factors”. In: *Przeglad gastroenterologiczny* 14.2 (2019), p. 89.

value = 0.56) ⁷. Recently, clinical standards (NICE protocol) that include colonoscopy devices with NBI (narrow band imaging) filter had allowed real-time optical diagnosis from a vascular patterns characterization ^{8, 7, 9}. Specifically, the NBI filters the wavelengths that correspond to hemoglobin absorption. This enhances blood vessel patterns, showing an increased adenoma detection rate (ADR) of 15.3%, regarding the optical colonoscopy (OC) analysis ¹⁰. This fact improves the positive patient survival rate, since with every 1% ADR improvement, the CRC-associated risk, and related mortality, decrease by 3% and 5%, respectively ⁴.

Nowadays, there is still no clear definition of the polyp vascular patterns and the stratification w.r.t to CRC ⁴. For instance, the expert observational polyp analysis, over NBI sequences, reports high interclass variability with a significant rate of false-positive mistakes (around 80% of serrated polyps are misclassified as hyperplastic) ¹¹. In this sense, computational approaches have emerged to support polyp classification, dealing with intra and inter-observational diagnosis variation, principally following deep representations. These approaches, however, operate on independent domains (trained independently with NBI or OC samples), which reduces the capability to use such representations on common clinical scenarios and losing integrated infor-

⁷ Francesco Cocomazzi et al. “Accuracy and inter-observer agreement of the nice and kudo classifications of superficial colonic lesions: a comparative study”. In: *International journal of colorectal disease* (2021), pp. 1–8.

⁸ Driffa Moussata et al. “Endoscopic and histologic characteristics of serrated lesions”. In: *World journal of gastroenterology: WJG* 21.10 (2015), p. 2896.

⁹ Tonya Kaltenbach et al. “Endoscopic removal of colorectal lesions—recommendations by the US Multi-Society Task Force on Colorectal Cancer”. In: *Gastroenterology* 158.4 (2020), pp. 1095–1129.

¹⁰ Irina Ioana Vișovan et al. “The role of narrow band imaging in colorectal polyp detection”. In: *Bosnian journal of basic medical sciences* 17.2 (2017), p. 152.

¹¹ Koichi Okamoto et al. “Clinicopathological characteristics of serrated polyps as precursors to colorectal cancer: current status and management”. In: *Journal of gastroenterology and hepatology* 32.2 (2017), pp. 358–367.

mation that may help with polyp characterization^{12, 13}. Besides, this analysis implies additional challenges related to sudden camera movements, bubbles, some blood, food waste, poor patient preparation, and the changing lighting conditions impacting the patient’s diagnosis⁴. Even worst, despite the increased use of NBI filters in the clinical routine, this tool is still limited to specialized or academic centers⁴.

This work introduces a deep generative representation with the capability to produce synthetic and enhanced optical images that include vascular patterns and allow discrimination among polyp classes. Interestingly, the proposed approach can take conventional colonoscopy observations, which are further enriched with NBI patterns, following translation tasks. The learning of the architecture is restricted from a cancer classification task and also a patch local condition to discriminate among synthetic and real sequences. The architecture is trained from an end-to-end scheme, achieving a remarkable separation into a coded embedding space representing each observed colonoscopy frame. Alternatively, the architecture generates synthetic NBI sequences that may support *in situ* analysis. During validation, the proposed architecture showed robustness to discriminate among adenoma and hyperplastic classes but also sensitivity to differentiate serrated samples (unseen during training). The partial content of this work has been accepted and published at the **44th Annual International Conference of the IEEE Engineering in Medicine and Biology Society (EMBC’22)**

¹² Jiawei Chen et al. “Generative adversarial networks for video-to-video domain adaptation”. In: *Proceedings of the AAAI Conference on Artificial Intelligence*. Vol. 34. 04. 2020, pp. 3462–3469.

¹³ Akihiro Fukuda et al. “Generating virtual chromoendoscopic images and improving detectability and classification performance of endoscopic lesions”. In: *Domain Adaptation and Representation Transfer and Medical Image Learning with Less Labels and Imperfect Data*. Springer, 2019, pp. 99–107.

1. FUNDAMENTALS

1.1. Clinical polyp characterization

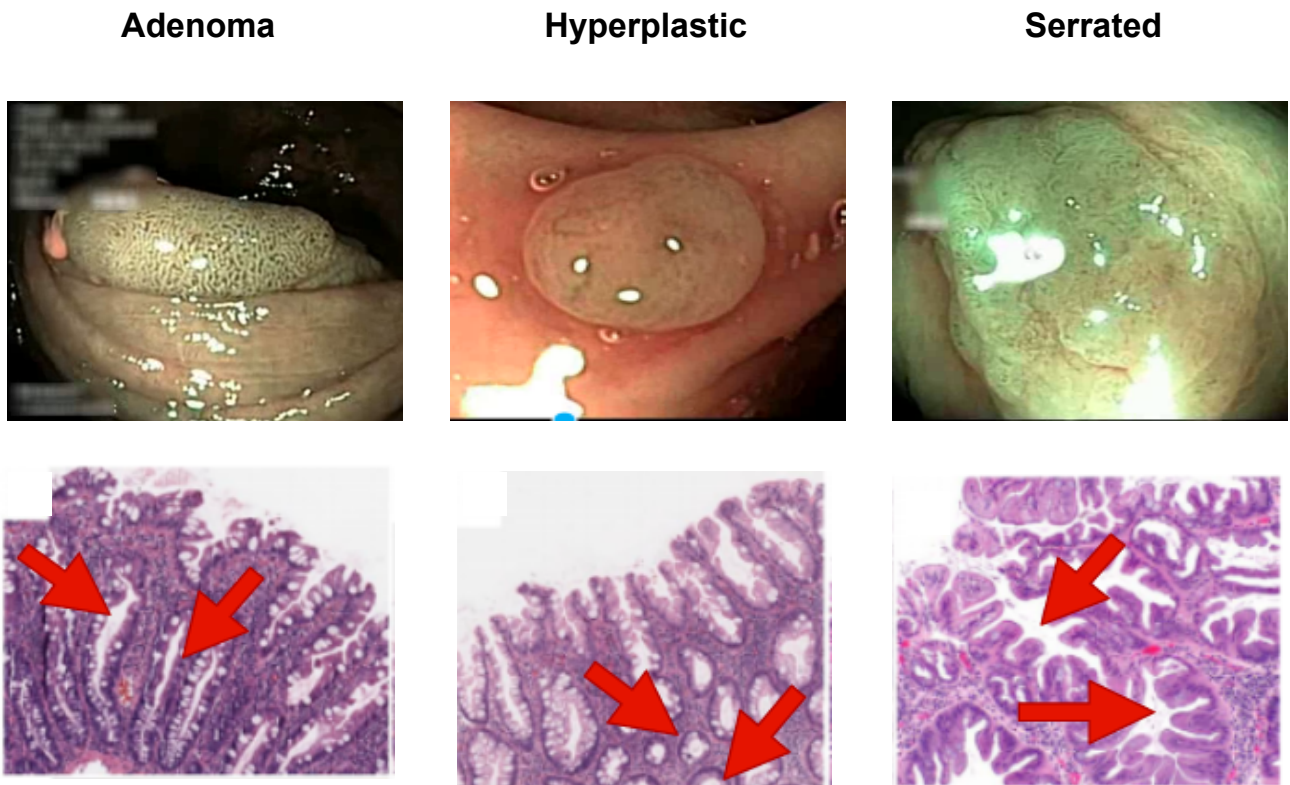
Polyps are the main biomarkers of CRC and their nature is completely asymptomatic. A polyp is an abnormal protrusion as the consequence of the growth of a group of cells of any membranous tissue. The early stages become a crucial factor for the patient's life, increasing the survival rate by up to 90% ⁶. The standard procedure for polyp detection is the colonoscopy, where the neoplastic (carcinogenic) grade is evaluated according to clinical protocols and eventually sent for histopathological studies.

From histopathology analysis, CRC polyps are classified into three types: hyperplastic, adenomas, and serrated samples. Hyperplastic polyps are mainly characterized by regular contour and round nuclei. Adenomas, on the other hand, contain closely spaced tubules, thin nuclei, and pseudo stratification. The serrated samples, show the presence of a serrated shape, mild nuclear stratification, a slight increase in cytoplasmic proportion, and elongated nuclei ¹⁴. Figure 1 shows the macroscopic and microscopic appearance of each type of polyp. Arrows point to the main microscopic features. The primary obstacle lies in achieving accurate polyp classification during colonoscopy procedures, which involves identifying patterns that can be subsequently validated through histopathological analysis. The classification from colonoscopies is an opportunity to early diagnose and stratify the CRC disease.

Macroscopically there exist three principal protocols to coarsely classify polyps according to different observations. The *Paris* protocol categorizes polyps according to their shape (flat,

¹⁴ Teri A Longacre and Cecilia M Fenoglio-Preiser. "Mixed hyperplastic adenomatous polyps/serrated adenomas. A distinct form of colorectal neoplasia." In: *The American journal of surgical pathology* 14.6 (1990), pp. 524–537.

Figure 1. Macroscopic and microscopic appearance for the three main types of polyps. Arrows point to closely spaced tubules, round nuclei, and serrated shapes for adenoma, hyperplastic, and serrated samples, respectively.



pendular, excavated, etc) but with lower correlations w.r.t. biopsy studies⁷. On the other hand, the *Kudo* protocol employs chromoendoscopy techniques improving the correct visual grading of up to 24.5% over the *Paris* protocol⁴. Nonetheless, the *Kudo* applicability involves a high cost regarding the specialized equipment and contrast substances¹⁵. For this reason, the *NICE* protocol has currently gained relevance, by coding vascular patterns as a differential factor between the different types of polyps. This protocol has reported correlation and accurate detection up to 93% regarding biopsy ground truth⁵. For doing so, this protocol uses NBI light

¹⁵ Pablo Mesejo et al. “Computer-aided classification of gastrointestinal lesions in regular colonoscopy”. In: *IEEE transactions on medical imaging* 35.9 (2016), pp. 2051–2063.

acquisitions, which improves the visibility of both mucosa and blood vessels. Particularly, this NBI light uses a near band filter to capture wavelengths related to the absorption spectrum of hemoglobin, *i.e.*, the incidence of particular wavelengths related to blood vessels but reflected in the mucosa. Despite marked advantages, this protocol remains subjective to properly define vascular pattern boundaries among poly classes ⁴. In particular, from the *NICE* protocol, the macroscopic polyp features are described as follows:

- **Adenomas** is the most proliferative polyp with associated carcinogenic characteristics ¹⁶. The size of this polyp class has a positive correlation with CRC, being at least the 50 % found in the rectum and ascending colon ¹⁶. The adenoma polyps are characterized by a marked microvascular pattern. Unfortunately, this detection rate is highly dependent on the degree of expertise of the specialist and other factors associated with the clinical practice, presenting a variation between 7 and 53% ¹⁷.
- **Hyperplastic** polyps are the second most frequent biomarker categorized as non-neoplastic lesions, a polypectomy procedure means unnecessary risks such as bleeding and perforation ¹⁸. Frequently, hyperplastic polyps appear at descending colon with sizes less than 10mm in diameter, where microvascular patterns are scarce with a smooth textural appearance ¹⁶. This group of intestinal lesions together with adenomas are the two groups of biomarkers that until now were widely known by specialists ¹⁴.
- **Serrated** polyps are currently of particular interest because they present mixed characteristics of the adenoma and hyperplastic samples. In particular, under magnified images,

¹⁶ Franziska Haumaier, William Sterlacci, and Michael Vieth. “Histological and molecular classification of gastrointestinal polyps”. In: *Best Practice & Research Clinical Gastroenterology* 31.4 (2017), pp. 369–379.

¹⁷ Gregor Urban et al. “Deep learning localizes and identifies polyps in real time with 96% accuracy in screening colonoscopy”. In: *Gastroenterology* 155.4 (2018), pp. 1069–1078.

¹⁸ Ruihai Zhang et al. “Automatic detection and classification of colorectal polyps by transferring low-level CNN features from nonmedical domain”. In: *IEEE journal of biomedical and health informatics* 21.1 (2016), pp. 41–47.

serrated polyps show intermediate mucus and microvascular patterns compared to adenoma and hyperplastic samples¹⁴. This particular fact is what makes serrated samples one of the potential candidates associated with a high degree of CRC development. Reports indicate that they are the precursors of approximately 30% of CRC cases¹¹. Previously, serrated masses were widely classified as hyperplastic and were not considered clinically relevant to the patient¹⁹, resulting in high rates of misclassification that consequently contributed to the high incidence and mortality rates worldwide.

Figure 2. Visualization of the main CRC biomarkers under conventional OC and NBI illumination sources. Each row shows the high intraclass variability whereas each column shows the vascular enrichment enhanced by using NBI light

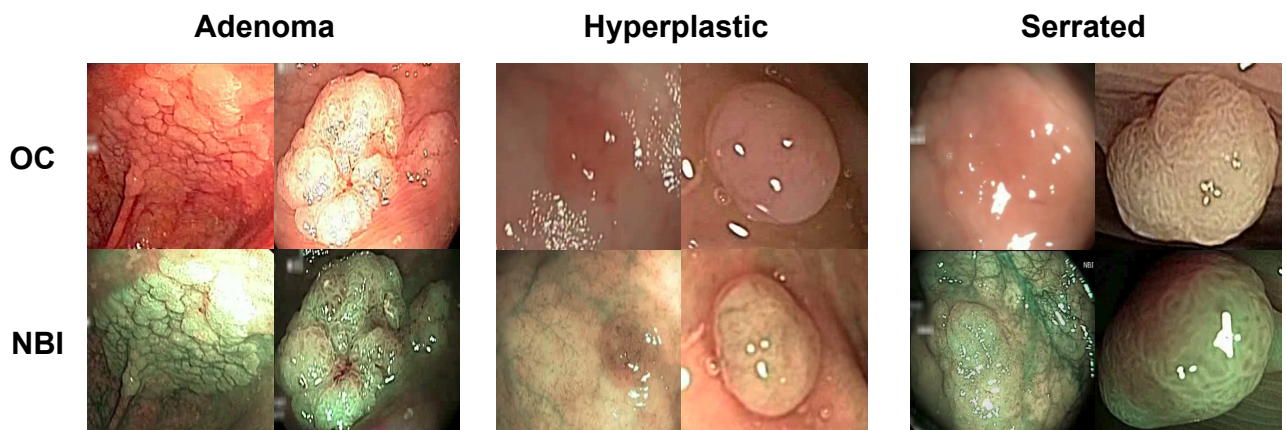


Figure 2 shows the typical appearance of each polyp type, acquired by both OC and NBI sources. The enhancement of features that are missed under OC is evident. Although the vascular pattern distinction on NBI sequences is becoming increasingly common in colonoscopy procedures, its use is still restricted to specialized centers as it is highly dependent on the experience and training of the clinical staff⁴. On the other hand, the rows evidence high inter-class similarity and high intra-class variability.

¹⁹ David H Kim et al. “Serrated polyps at CT colonography: prevalence and characteristics of the serrated polyp spectrum”. In: *Radiology* 280.2 (2016), pp. 455–463.

1.2. Computational approaches to characterize polyp malignancy

Currently, computational approaches seek optical characterization and diagnosis to determine the selective resection of neoplastic polyps. Recently, this task has become more effective with specialized optical imaging techniques such as NBI sequences, which enable the visualization of microvascular patterns specific to each biomarker type. Nevertheless, these approaches can vary according to the training rule, following a purely discriminatory task or using the synthesis image generation as a pretext task. In brief, these methodologies are exposed in the next subsections.

1.2.1. Classification methods Nowadays, computer-aided diagnostic systems (CAD) are used during colonoscopy procedures to support the detection and classification of colorectal polyps.

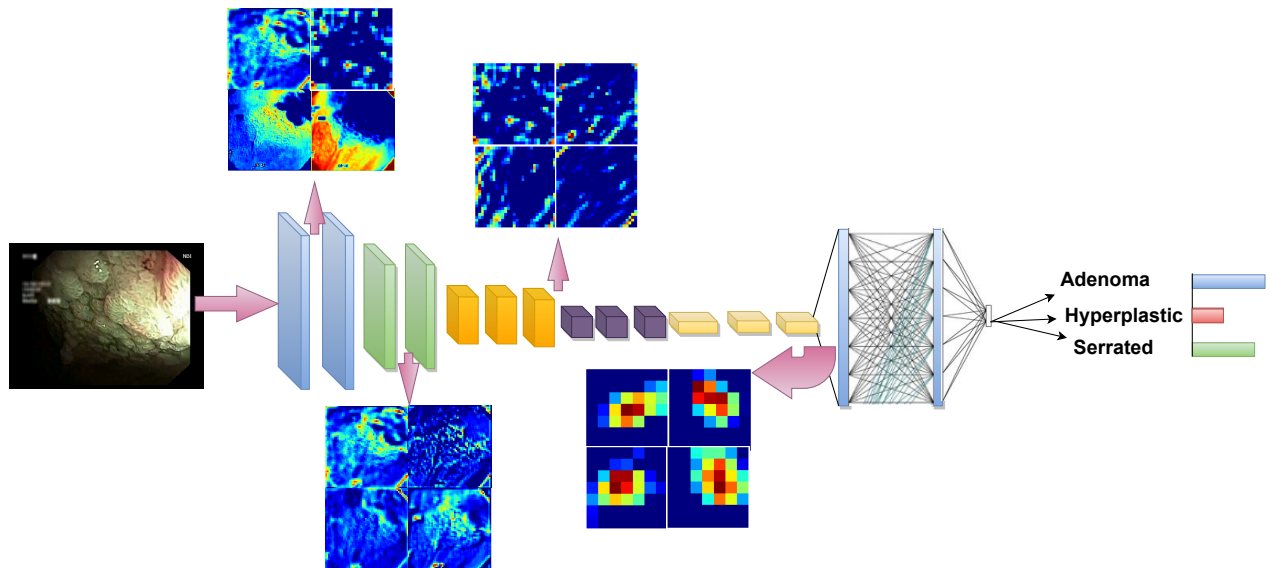


Figure 3. CAD system representation in which hierarchical feature extraction is achieved from an input image, allowing the biomarker prediction.

These systems have shown remarkable improvement in diagnosis, reducing the loss and misclassification of polyps during clinical procedure ²⁰. Recently, deep learning strategies have shown great contributions in the development of CADs systems supporting the characterization and diagnosis of polyps ⁴. This new learning scheme focuses on hierarchical feature extraction through convolutional layers. The purpose of a convolutional layer is to extract primary spatial patterns such as textures, which are in turn the input for successive convolutional layers until a semantic relationship in the top layers. Figure 3 provides a general outline of this concept. This semantic relationship corresponds to the model's prediction.

1.2.2. Generative mechanisms as biomarker descriptors New alternatives of deep learning such as generative architectures may supply a lack of sufficient data and also they may be robust to weak and biased annotations. In such mechanisms, the self-supervised fit the deep representation by using visual information of input training samples. For instance, image translation task try to align domain $X = \{x_1, x_2, \dots, x_n\}$, and the domain $Y = \{y_1, y_2, \dots, y_m\}$, without necessary coincidence, *i.e.* $\dim(X) \equiv n \neq \dim(Y) \equiv m$. This task is currently solved with *Cyclegan* algorithm (figure 4) that allows an image-to-image translation between unaligned domains ²¹. That is, element of the set x_i there is no corresponding representation y_i and vice versa. This fact makes this algorithm a potential alternative in clinical practice where poor domain alignment is the common scenario. This inter-domain translation task will be used as a pretext task where we hypothesize the ability of the algorithm to extract typical latent representations of the domains to be treated. Its operation is detailed in a simple version below. In this particular case, it is defined as two sets as X y Y . The transformation function $\delta(x) : X \longrightarrow Y$ is a generator mathematically defined as an injective function $\delta(x_i) = \hat{y}_i / \hat{y}_i \approx y$. This similarity relationship is evaluated by a discriminator matching w.r.t the target domain. Due to

²⁰ Yuichi Mori et al. “Computer-aided diagnosis for colonoscopy”. In: *Endoscopy* 49.08 (2017), pp. 813–819.

²¹ Jun-Yan Zhu et al. “Unpaired image-to-image translation using cycle-consistent adversarial networks”. In: *Proceedings of the IEEE international conference on computer vision*. 2017, pp. 2223–2232.

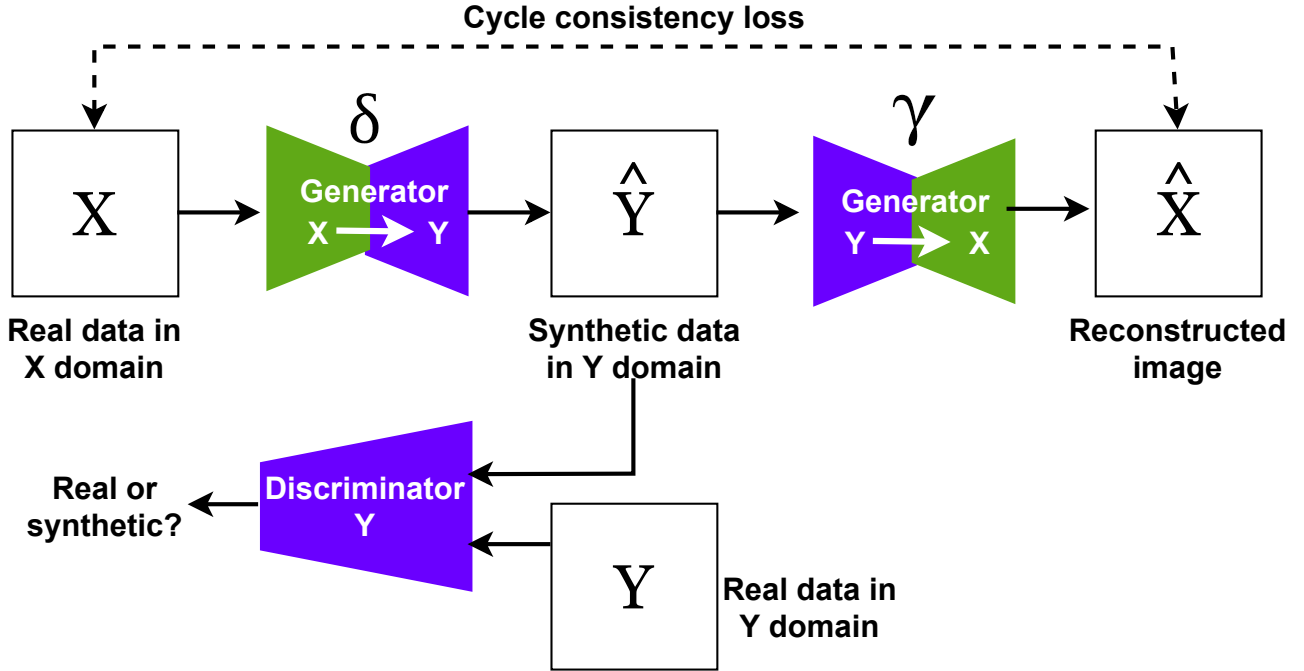


Figure 4. Cyclegan architecture uses non-aligned samples to achieve domain translation. A discriminative network differentiates the synthetic and real data, while a cycle-consistent loss ensures that the reconstruction is accurate.

the un-paired source and target domains, this cross-domain translation may cause meaningless reconstructions (hallucinations)²². To address this problem, it is defined as a generator that reverts the reconstruction to the starting domain to guarantee reconstructions on the source sample, i.e., the transformation function that reverts $\delta(x)$ defined as $\gamma(y) : Y \rightarrow X$. In particular, this inverse function is defined as $\gamma(y_i) = \hat{x}_i / \hat{x}_i \approx x$. The similarity between the inverse mapping given by the γ function and the source sample is known as a cycle-consistent loss defined as:

²² Joseph Paul Cohen, Margaux Luck, and Sina Honari. “Distribution matching losses can hallucinate features in medical image translation”. In: *Medical Image Computing and Computer Assisted Intervention–MICCAI 2018: 21st International Conference, Granada, Spain, September 16–20, 2018, Proceedings, Part I*. Springer. 2018, pp. 529–536.

$$L_{cyc}(\delta, \gamma) = \mathbb{E}_{X \sim P_{data}(X)} [\|\gamma(\delta(X)) - X\|_1] + \mathbb{E}_{y \sim P_{data}(Y)} [\|\delta(\gamma(Y)) - Y\|_1]$$

The above expression is the loss function defined in the *Cyclegan* algorithm, which looks for the differences between the 'synthetic' translations and the 'real' domains given by the L1 norm. The L1 norm also known as *Manhattan* distance, measures the absolute distance between the elements of each vector. As a result, unsupervised learning may be used to perform translations across unaligned domains. This strategy may be employed as a pretext task to learn complex colonoscopy patterns that are necessary to represent videos in both domains. The result is an enriched representation that follows a weakly supervised training and code polyp representation in embedding vectors, learned from the translation task. The resultant embedding representation may compactly represent input video sequences and therefore built a geometrical low-dimensional space, from which is possible to achieve the classification of polyps. For instance, the input of OC or NBI sequences may be mapped to translation architecture, and the returned embedding vectors are the descriptors to classify polyp classes. Alternatively, the translation scheme may be used to map OC sequences and obtain NBI images that are enriched with vascular representation and may contribute to the polyp classification.

1.3. Related work

The neoplastic/hyperplastic polyp characterization task has been explored from classical machine learning strategies to deep convolutional representations as polyp descriptors extractors

²³, ²⁴, ²⁵. Polyp features such as texture, color, and 3D morphology; have been used as descriptors to discriminate between adenoma, hyperplastic and serrated samples ²⁶. Several strategies have been dedicated to characterizing polyp vascular patterns taking advantage of NBI sources. For instance, Horiuchi et al. modeled NBI sequences from a GoogLeNet architecture to classify between early carcinogenic patterns and gastritis regions ²⁷. Despite using NBI and OC, these methods are camera-sensitive and require controlled conditions, which are unrealistic in clinical practice. Transfer learning technique used in ResNet50 and Inception v3 architectures to classify healthy/neoplastic polyps from NBI sequences in the Ueyama et al. and Chen et al works, respectively ²⁸, ²⁹. Despite these efforts, these approaches remain limited to classifying serrated intermediate patterns, which could be crucial in the early stages of the disease ¹¹. The deep representation has also been adjusted over OC sequences but with limitations associated

-
- ²³ Sebastian Gross et al. “Computer-based classification of small colorectal polyps by using narrow-band imaging with optical magnification”. In: *Gastrointestinal endoscopy* 74.6 (2011), pp. 1354–1359.
- ²⁴ Lan Li et al. “Convolutional neural network for the diagnosis of early gastric cancer based on magnifying narrow band imaging”. In: *Gastric Cancer* 23 (2020), pp. 126–132.
- ²⁵ Hiroyasu Usami et al. “Colorectal polyp classification based on latent sharing features domain from multiple endoscopy images”. In: *Procedia Computer Science* 176 (2020), pp. 2507–2514.
- ²⁶ Kristijan Cincar and Ioan Sima. “Machine Learning algorithms approach for Gastrointestinal Polyps classification”. In: *2020 International Conference on INnovations in Intelligent SysTems and Applications (INISTA)*. IEEE. 2020, pp. 1–6.
- ²⁷ Yusuke Horiuchi et al. “Convolutional neural network for differentiating gastric cancer from gastritis using magnified endoscopy with narrow band imaging”. In: *Digestive diseases and sciences* 65 (2020), pp. 1355–1363.
- ²⁸ Hiroya Ueyama et al. “Application of artificial intelligence using a convolutional neural network for diagnosis of early gastric cancer based on magnifying endoscopy with narrow-band imaging”. In: *Journal of gastroenterology and hepatology* 36.2 (2021), pp. 482–489.
- ²⁹ Peng-Jen Chen et al. “Accurate classification of diminutive colorectal polyps using computer-aided analysis”. In: *Gastroenterology* 154.3 (2018), pp. 568–575.

with loss of input vascularity observations³⁰. In addition, standard deep architectures have been adjusted to support polyp resection decisions with polyp segmentation masks³¹. These end-to-end approaches have been dedicated to independent image modalities, losing sharing information and important applicability in standard clinical contexts. Additional studies have classified adenomas, hyperplastic and serrated classes in controlled scenarios with high-quality image acquisitions. Nevertheless, despite the high-quality image restriction, the achieved results are lower than the corresponding NBI sequences³². Nonetheless, such NBI representations are nowadays restricted to specialized or academic centers⁴. Recent approaches have used image translation to classify polyps by mapping vascular NBI patterns. For doing so, a teacher-student convolutional architecture and a vision transformer scheme were updated to achieve textural translation from NBI to OC sequences, but they require strict alignment, which is unrealistic in real scenarios^{33, 34}.

³⁰ Young Joo Yang et al. “Automated classification of colorectal neoplasms in white-light colonoscopy images via deep learning”. In: *Journal of clinical medicine* 9.5 (2020), p. 1593.

³¹ Eladio Rodriguez-Diaz et al. “Real-time artificial intelligence-based histologic classification of colorectal polyps with augmented visualization”. In: *Gastrointestinal Endoscopy* 93.3 (2021), pp. 662–670.

³² Tsuyoshi Ozawa et al. “Automated endoscopic detection and classification of colorectal polyps using convolutional neural networks”. In: *Therapeutic advances in gastroenterology* 13 (2020), p. 1756284820910659.

³³ Qin Wang et al. “Colorectal Polyp Classification from White-Light Colonoscopy Images via Domain Alignment”. In: *International Conference on Medical Image Computing and Computer-Assisted Intervention*. Springer. 2021, pp. 24–32.

³⁴ Weijie Ma et al. “Toward Clinically Assisted Colorectal Polyp Recognition via Structured Cross-Modal Representation Consistency”. In: *International Conference on Medical Image Computing and Computer-Assisted Intervention*. Springer. 2022, pp. 141–150.

2. RESEARCH PROBLEM

Colorectal cancer (CRC) is the third most common type of cancer and the second in mortality worldwide². A correct and early polypectomy of neoplastic tumors increases 90% the survival rate⁶. Clinically, an early diagnosis is achieved by searching and categorizing abnormal polyp masses from an exhaustive evaluation in a colonoscopy procedure. These polyps are categorized as hyperplastic (without clinical risk), neoplastic adenoma, which represents 70% of lesions, and more recently, the serrated category that shares adenomas and hyperplastic features, and it may be a potential biomarker for early diagnosis^{16, 14}. The discrimination of such categories is mainly based on vascular patterns, which result very limited in standard optical colonoscopies (OC-white light). Some studies report a moderate agreement to classify polyps in OC of around 0.61 in kappa value⁷. More specialized colonoscopies have recently integrated NBI sequences that allow an enriched observation of vascular patterns concerning OC, outperforming classification until 20%^{5, 10}. Nonetheless, this classification remains subjective, dependent on expert observations, reporting a moderate agreement among gastroenterologists (Kappa of 0.65)³⁵ but also reporting a significant rate of false-positive mistakes¹⁹.

Computational tools have emerged as an alternative to support polyp characterization and classification. Some of these approaches have been proposed over typical OC colonoscopies because of the availability of standard routines. These most outstanding strategies are based on the convolutional representation that properly localizes polyps but remains limited in the classification task. Despite of hierarchical representation of these nets, the poor vascular patterns observed from such OC sequences limit the discrimination capability of the methods⁵. Hence, computational approaches that operate over NBI sequences have properly dealt with the extreme

³⁵ Eun Mi Song et al. “Endoscopic diagnosis and treatment planning for colorectal polyps using a deep-learning model”. In: *Scientific reports* 10.1 (2020), pp. 1–10.

classification of polyps (adenoma vs hyperplastic) but using crop and controlled input sequences³⁶. These approaches have allowed to support polyp characterization but the specialized requirements of narrow band filters limit the implementation on clinical routine. Besides, these deep representations are namely based on discriminative rules that require a stratified dataset, with a significant amount of samples for each considered class. More recently approaches have tried to capture the vascular pattern from NBI and project such representation into OC colonoscopies. In such cases, the approach takes advantage of NBI representation but operates on OC colonoscopies, which results in powerful issues to transfer strategies on most common clinical scenarios. Nonetheless, preliminary studies have proposed architectures that depend on paired NBI-OC sequences, observing the same polyp observations^{33, 34}. This scheme is tedious and limits the training representation to sophisticated protocols to capture tuple samples. Also, this particular training scheme maybe leads to overfitted representation that learns particular intestinal fold correlation in both sources more than vascular codification.

2.1. Research question

How to characterize *in situ* polyp vascular patterns correlated with the degree of malignancy of the CRC?

Hypothesis:

Generative learning mechanisms could offer an alternative mechanism to codify non-aligned hidden descriptors and approximate vascular narrow polyp patterns from standard colonoscopy sequences.

³⁶ Cristina Sánchez-Montes et al. “Computer-aided prediction of polyp histology on white light colonoscopy using surface pattern analysis”. In: *Endoscopy* 51.03 (2019), pp. 261–265.

3. OBJECTIVES

3.1. General objective

To develop a generative deep translation scheme to characterize polyp NBI vascular patterns in white light sequences.

3.2. Specific objectives

- To select a dataset that includes sequences in NBI and white light domain, labeled with polyp classes, according to a biopsy study.
- To develop a deep generative architecture that can translate among two light colonoscopy sources.
- To validate the proposed approach to the capability to classify polyps and generate enriched white colonoscopy sequences.
- To project hidden deep vectors of the generative net into a low-dimensional space to discriminate among polyp classes.

4. PROPOSED APPROACH

In this work, we adopted a Cyclegan image-to-image translation to recover the most related NBI sequence from a standard OC sequence input, which potentially coded digital biomarkers highly correlated with CRC malignancy degrees. This architecture was constrained to learn specific cancer class distributions from a polyp classification convolutional net, allowing a more consistent embedding space. Also, to guarantee NBI/OC distribution consistency, a *PatchGan* discriminatory network was integrated to measure the match distribution from synthetic and real data distributions. The general pipeline of the proposed approach is illustrated in figure 5. The complete content of this section has been accepted in "The IEEE Engineering in Medicine and Biology Society" international conference ³⁷ and it is under review for the Biomedical Informatics journal ³⁸.

³⁷ Franklin Sierra-Jerez, Jair Ruiz, and Fabio Martínez. “A Non-Aligned Deep Representation to Enhance Standard Colonoscopy Observations from Vascular Narrow Band Polyp Patterns.” In: *2022 44th Annual International Conference of the IEEE Engineering in Medicine & Biology Society (EMBC)*. IEEE. 2022, pp. 1671–1674.

³⁸ <https://www.sciencedirect.com/journal/journal-of-biomedical-informatics>

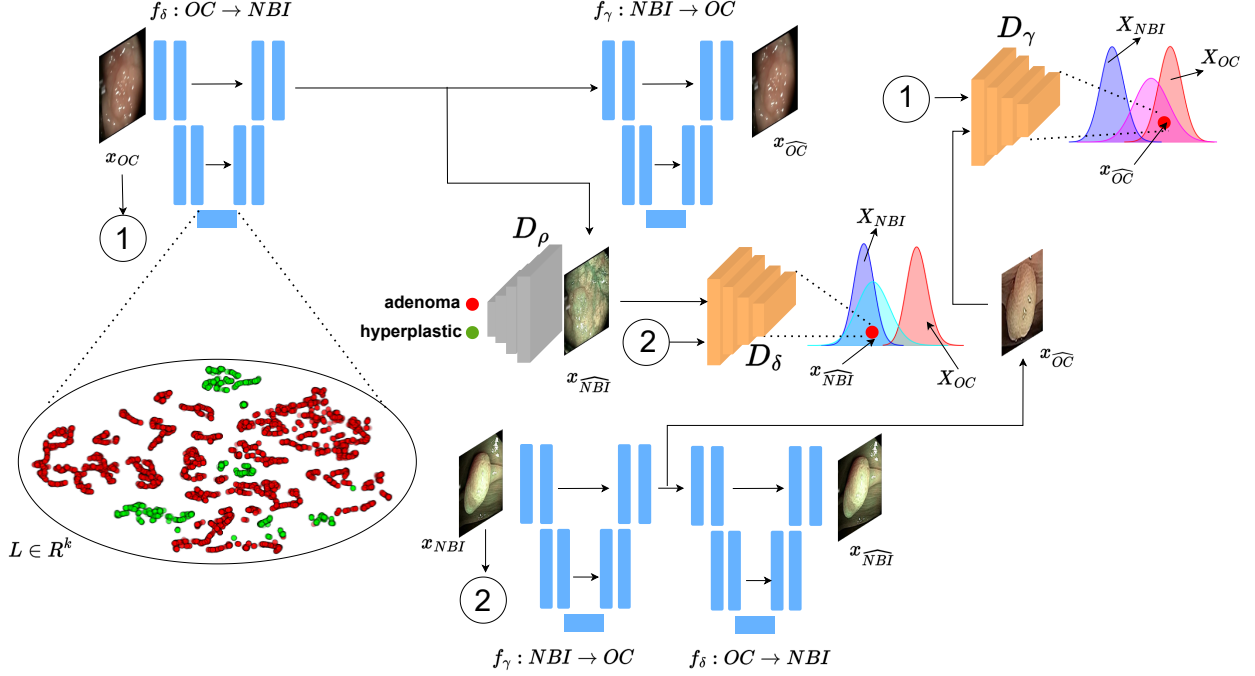


Figure 5. Multitask polyp image translation-classification proposed approach. The bidirectional OC-NBI and NBI-OC representations are encoded by \mathbf{f}_δ and \mathbf{f}_γ generators, respectively. D_δ and D_γ discriminators ensure the proper source domain adaption. Typical OC sequences are enhanced with related NBI vascular patterns and automatically classified as adenoma or hyperplastic samples. Adenoma-hyperplastic NBI patterns are embedded in the \mathbf{f}_δ generator space representation serving as a malignancy discriminator visual aid".

4.1. Polyp vascular features mapping from NBI to OC

Here, vascular polyp patterns (from NBI) are projected to optical colonoscopies (OC) observations to enhance polyp representation. For doing so, a non-aligned self-representation is implemented from a couple of generative networks (\mathbf{f}_δ , \mathbf{f}_γ ; with respective $\boldsymbol{\delta}$, $\boldsymbol{\gamma}$ weights). The \mathbf{f}_δ generator learns typical NBI patterns, while the \mathbf{f}_γ generator updates an "inverse function" to recover the original OC sequences from the synthetic \mathbf{f}_δ outputs. In the second training stage, the \mathbf{f}_δ generator receives synthetic OC frames, while the \mathbf{f}_γ generator receives real NBI observations. These nets are updated through a cycle consistency loss²¹ ensuring the reversed projection to the original representation, following the expression:

$$L_{cyc}(\mathbf{f}_\delta, \mathbf{f}_\gamma) = \mathbb{E}_{\mathbf{x}_{OC} \sim P_{data}(\mathbf{x}_{OC})} [\|\mathbf{f}_\gamma(\mathbf{f}_\delta(\mathbf{x}_{OC})) - \mathbf{x}_{OC}\|_1] + \mathbb{E}_{\mathbf{x}_{NBI} \sim P_{data}(\mathbf{x}_{NBI})} [\|\mathbf{f}_\delta(\mathbf{f}_\gamma(\mathbf{x}_{NBI})) - \mathbf{x}_{NBI}\|_1] \quad (1)$$

where $\mathbf{f}_\gamma(\mathbf{f}_\delta(\mathbf{x}_{OC})) \approx \mathbf{x}_{OC}$, $\mathbf{f}_\delta(\mathbf{f}_\gamma(\mathbf{x}_{NBI})) \approx \mathbf{x}_{NBI}$ ensures that colonoscopy sequences recreation remain in real data distributions $\mathbf{X}_{OC}, \mathbf{X}_{NBI}$. In this work, the translation nets $(\mathbf{f}_\delta, \mathbf{f}_\gamma)$ are implemented as Unet convolutional version, allowing morphological structure preservation through the skip connections and the monitoring of reconstruction through different levels, by concatenating inputs of the decoder in the decoder path.

Complementary, a couple of *PatchGan* discriminatory networks evaluate the reconstruction domain fidelity for both NBI and OC sources (see an illustration of domain distributions in Figure 5). From such implementation, OC sequences enhanced with typical NBI polyp vascular patterns can be obtained without the aligned-domain restriction. To force the embedding representation to encode micro-vascular patterns, this scheme is complemented with a polyp classification net (\mathbf{D}_p , with weights p) to discriminate enhanced OC sequences between adenoma and hyperplastic diagnoses. This classification net (\mathbf{D}_p) is adjusted from a typical cross-entropy loss as $L_{D_p} = y \log(\hat{y})$. In such a case, each synthetic NBI sequence serves as input for this convolutional neural network (\mathbf{D}_p). It should be noted that such a model is integrated with the generative scheme impacting also the synthetic image representation. To achieve enhanced but also discriminative OC sequences, the \mathbf{f}_δ synthesis is updated as:

$$L_{\mathbf{f}_\delta} = L_{OC \rightarrow \hat{NBI}} + L_{cyc} + L_{NBI \rightarrow \hat{NBI}} \quad (2)$$

where the L_{cyc} is from equation 1. The $L_{OC \rightarrow \hat{NBI}}$ minimize error regarding the capability to reconstruct \hat{NBI} patterns from OC , which is defined as:

$$L_{OC \rightarrow NBI} = \mathbb{E}_{x_{NBI} \sim P_{\text{data}}(\mathbf{x}_{NBI})} [\log D_\delta(x_{NBI})] + \mathbb{E}_{x_{OC} \sim P_{\text{data}}(\mathbf{x}_{OC})} [\log(1 - D_\delta(\mathbf{f}_\delta(x_{OC})))] \quad (3)$$

The $L_{NBI \rightarrow NBI} = \mathbb{E}_{\mathbf{x}_{NBI} \sim P_{\text{data}}(\mathbf{x}_{NBI})} [\|\mathbf{f}_\delta(\mathbf{x}_{NBI}) - \mathbf{x}_{NBI}\|_1]$ is also called *identity loss* that preserves the color composition between domains and measures the consistency of polyp morphology. The same minimization rule $L_\gamma = L_{NBI \rightarrow OC} + L_{cyc} + L_{OC \rightarrow OC}$ is applied for the \mathbf{f}_γ generator. Hence, the full objective rule for the complete minimization is defined, as:

$$L_{total}(\mathbf{f}_\delta, \mathbf{f}_\gamma, D_\delta, D_\gamma, y) = L_{\mathbf{f}_\delta} + L_{\mathbf{f}_\gamma} + L_{cyc}(\mathbf{f}_\delta, \mathbf{f}_\gamma) + L_{D_\rho} \quad (4)$$

4.2. An embedding polyp-class representation

From the adjusted representation, the proposed approach recovers a latent embedding space from the \mathbf{f}_δ generator. Each embedding vector is recovered from each polyp observation (x_i^{OC}) producing a synthetic NBI observation $\mathbf{f}_\delta(x_n^{OC}) \rightarrow \hat{x}_n^{NBI}$. The set of low-dimensional embedding vectors $\mathbf{L} = \{l_1, l_2, \dots, l_n\}; l_i \in R^k$ form a geometrical space, that may be discriminative regarding the adenoma and hyperplastic classes. Each encoding vector l_i is formed by k scalar values. In such a case, we can operate over such embedding space, projecting new OC observations and recovering the CRC degree, according to the neighboring relationship.

Embedding visual projection. The \mathbf{f}_δ geometric space could be seen as an aid visual tool that may be projected into a two-dimensional representation through a T-sne (t-distributed Stochastic Neighbor space) that preserves the high-dimension embedding data structure. To emulate the geometric data distribution into a low dimensional space, each embedding vector l_i is compared against each point in the \mathbf{L} set. These distances are coded as conditional probabilities to represent the similarity in each pair of data points. The conditional probability of point \hat{l}_j to be next to the point \hat{l}_i is represented by a Gaussian distribution centered at \hat{l}_i and vari-

ance are given by the perplexity hyperparameter. From these conditional distributions, a joint probability distribution is measured taking into account the pairwise similarity $l_j^i = l_i^j$. Hence, a corresponding t-student distribution is computed from points with two or three dimensions. Hence, the Kullback-Leiber divergence is used to measure the difference between two probability distributions. From an iterative process, the T-sne uses gradient descent to achieve a fit of the t-student distribution to the original Gaussian distribution, following the Kullback-Leiber divergence.

5. EXPERIMENTAL SETUP

5.1. Data

The proposed approach was validated over a public dataset³⁹ with standard optical colonoscopies (OC), and the respective NBI sequences. The polyps are recorded from different perspectives, and following zoom-in and zoom-out exploration, resulting in observations with high textural and shape variations. These short video sequences are captured during a typical colonoscopy procedure, from which, the expert first navigates through the intestinal tract to find abnormal masses, *i.e.*, the polyps. This navigation is carried out from standard OC, and once the polyp is localized, the source is changed to NBI to follow a vascular inspection. Because this procedure is dynamic and the camera change of position to the change of light sources, we consider such sequences mainly unpaired. The closest paired information is only concentrated among frames that record the switching process. This dataset is composed of 76 short colonoscopy videos (30 seconds on average) with an image resolution of 768×576 pixels. Each observed polyp was labeled, according to biopsy results, and has the committee opinion of 4 experts and 3 beginners (a medical expert is a professional with more than eight years in colonoscopy procedures, and, a beginner participant has four or fewer years of experience in colonoscopy procedures). In summary, the recorded data has a distribution of a total of 40 adenomas, 21 hyperplastic, and 15 serrated polyp lesions.

As an extra validation, this work also includes a reduced subset of OC-NBI (from the same public dataset), that in the literature is reported as a paired, after a carefully expert selection of video clips³³. From such a subset was carry out a reconstruction validation among sequences, complements the discussion about the advantages and limitations of implemented architecture.

³⁹ http://www.depeca.uah.es/colonoscopy_dataset/

Also, we collect a set of four owner colonoscopies, that include OC and NBI observations of adenoma polyps. These videos were recorded in collaboration with *Instituto de Gastroenterología y Hepatología del Oriente - IGHO S.A.S, Bucaramanga, Colombia*. From such sequences, it was to do an initial estimation of the generalization capability of the proposed approach.

As reported in the literature, the serrated polyps have shared adenoma and hyperplastic features, whose labeling is highly biased by expert opinion^{16, 18}. Hence, for training purposes, the architecture was adjusted to discriminate between adenoma and hyperplastic samples. Then, 80% of adenoma and hyperplastic samples were taken for training the architecture, and 20% were reserved to test the discrimination of both classes. Moreover, the serrated subset was also used in this work but for testing purposes to determine the sensibility of the proposed approach, regarding such intermediate class. In such cases, serrated samples are totally unseen during architecture adjustment and only for testing purposes is retrieved the probability to belong to the adenoma class.

Image translation quality measures. An extra validation was carried out over a controlled subset to measure the quality of image synthesis obtained from translation tasks. For this reason, the adenoma and hyperplastic OC-NBI colonoscopy sequences were aligned to measure the OC-to-NBI image-to-image translation quality. This dataset covers 101 adenomas and 63 hyperplastic samples in each modality. To measure the image-to-image translation quality the following metrics were used:

- **PSNR.** The peak signal-to-noise ratio (PSNR) is a metric that measures the level (or ratio) between the desired image and the background noise expressed in decibels. In this sense, a high PSNR generally means a high image quality. The PSNR calculation is made by the mean squared error (MSE) and the maximum pixel value of the image (MAX_I) as follows: $PSNR = 10 \log_{10} \left(\frac{MAX_I^2}{MSE} \right)$
- **SSIM.** This metric tries to emulate human visual perception to identify the structural

information from a picture. The SSIM metric involves three metrics from an image: **luminance** $l(x, y)$, **contrast** $c(x, y)$, and **structure** $s(x, y)$ with $\alpha \geq 0$, $\beta \geq 0$, and $\gamma \geq 0$ to denote the importance of each metric as follows:

$$SSIM(x, y) = [l(x, y)]^\alpha \cdot [c(x, y)]^\beta \cdot [s(x, y)]^\gamma$$

- **M-SSIM.** This metric is an extension of the SSIM metric that results from the average SSIM performance computed over different regions, expressed as:

$$MSSIM(x, y) = \frac{1}{M} \sum_{i=1}^M SSIM(x_i, y_i)$$

5.2. Model setup

The proposed approach has the capability to translate from OC to NBI domain, allowing retrieval of synthetic OC-enhanced maps. From this translation scheme, it was also possible to encode embedded descriptors with the capability to discriminate among adenoma and hyperplastic classes. Regarding the translation task, the backbone was implemented with an *Unet* block for f_δ generator for the $OC \rightarrow NBI$ mapping. In the same way, an *Unet* block was implemented to f_γ generator for the $NBI \rightarrow OC$ reverse translation. Additionally, a *PatchGan* net is included in the end-to-end scheme to ensure a coherent domain adaptation. The description of the architecture is described as follows:

- A couple of *Unet* blocks have contractive and expansive paths that ensure textural preservation during learning. In our case, each block is implemented with 16 layers and 54.4 million parameters
- The PatchGan is a convolutional net with four convolutional layers with a number of kernels: 64-128-256-512. The total net has a total of 2.7 million parameters. The kernel size was set at 4 and the weights were initialized from a Gaussian distribution with values of 0 and 0.02 for mean and standard deviation, respectively. Unlike conventional discriminator in GANs schemes, the *PatchGan* architecture differentiate the generated distribution from

the original data distribution in a patch pixels average analysis. In this sense, *PatchGan* network is useful for image structure analysis distribution against conventional GANs discriminator⁴⁰.

- The proposed approach also includes a convolutional setup for polyp image classification. In such case, a VGG16 was implemented and previously trained over the training subset of NBI sequences.

Two different method configurations were here considered according to the adjustment of architectures. A first approximation focuses only on learning the translation domain without a classification ensemble. In a second approximation, the polyp classification was ensembled into a translation net to better adapt embedding space. During training, the complete architecture was adjusted with an Adam optimizer with a learning rate of 2×10^{-4} . The multitask proposed strategy was trained with 1200 frames from both light sources. The model image input is 256×256 with 50 epochs. Once adjusted the architecture, the embedding vectors were taken from the \mathbf{f}_δ block with a total size of 4096 scalar values. These embedding vectors are digital biomarkers capable of discriminating among observed classes. For classification, a simple KNN was implemented, varying K from 5 to 50. With this in mind, this topological vascular descriptor could be seen as an aid visual tool that may be useful in the medical opinion following a neighbor frame analysis across potential neoplastic areas.

⁴⁰ Phillip Isola et al. “Image-to-image translation with conditional adversarial networks”. In: *Proceedings of the IEEE conference on computer vision and pattern recognition*. 2017, pp. 1125–1134.

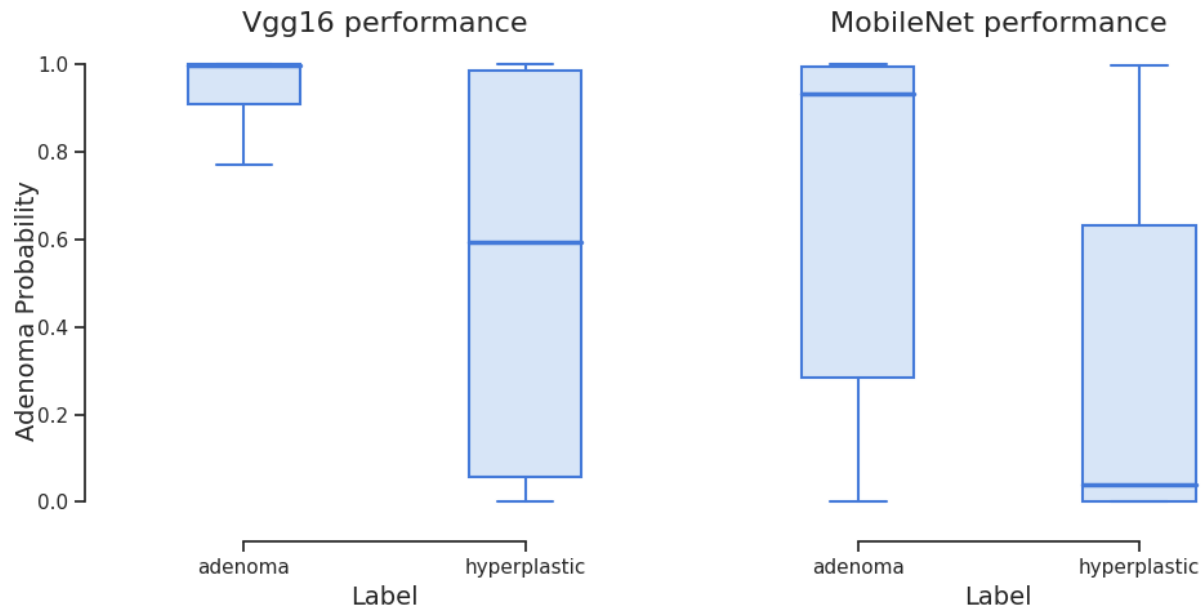
6. EVALUATION AND RESULTS

An ablation study was first carried out by setting adenoma vs hyperplastic classification from different convolutional backbones. This evaluation was carried out over a test subset (around 5476 and 5538 frames of 12 different videos from OC and NBI sources, respectively). The table on top of figure 6 summarizes classification scores, evidencing an outperforming for *Vgg16*, probably due to basic convolutional operations that preserve the image structure and morphological polyp features useful for a polyp-vascularity differentiation. Other compact convolutional backbones achieve remarkable discrimination results but the results suggest that deep-wise convolutions, inverted residuals, and compact blocks may introduce some numerical variations that limit the polyp characterization.

Figure 6 bottom shows the related adenoma probability distribution outputs for the two best-performing classification backbones over the adenoma and hyperplastic test samples. The box-plots show the adenoma probability distribution output of each model (y-axis) over all the test frames (adenomas and hyperplastic) on the x-axis. In this regard, we expect to have low probability outputs for hyperplastic samples, while high probability outputs for adenomas samples. As expected, the *Vgg16* achieves confident results with low dispersion to predict the neoplastic class. Interestingly, the probability of hyperplastic observations concerning the adenoma probability is dispersed when it should be noise and tend to be zero. This fact could be due to the class imbalance and might explain the poorest results against the other backbones in the precision metric. Regarding the *MobileNet* network, there is evidenced major dispersion of predicted samples, where probabilities are spread through all the possible values (high variability). Nonetheless, for the hyperplastic class, there are a few samples classified as adenomas samples (low false positive rate) that explain the achieved competitive precision metric (0.88%).

Figure 6. Ablation study over the test set for the polyp classification task. Graphics show the two best-performing networks for predicting the adenoma-related probability.

Model	Accuracy	Precision	Recall	F1-score
EfficientNet	0.67	0.87	0.67	0.76
Mobilenet	0.7	0.88	0.7	0.78
Vgg16	0.74	0.82	0.83	0.82



Once validated the capability of backbones to carry out classification, a second experiment consists on evaluate the discrimination capability of the proposed approach following a translation training scheme. In this case, we considered two classification options from the translation deep scheme. On the one hand, the output synthetic images (enhanced optical frame) were mapped to the D_ρ polyp classifier. On the other hand, the embedding descriptor is computed from \mathbf{f}_δ encoder, and then a classification is carried out from a KNN ($k=5$) strategy. The quantitative results for both classification options, from the translation scheme, are reported in table 1. Such comparison is also taking into account the results achieved by gastroenterologists (experts and beginners), the performance of raw OC and NBI sequences, the performance over the only translation task, and the classifier ensemble methods for the neoplastic prediction over synthetic frames and \mathbf{f}_δ embedding descriptors, respectively. As expected, both synthetic images achieve remarkable classification scores, outperforming the discrimination from typical OC sequences by 24% and 30% for the only translation task and the classifier ensemble, respectively. Interestingly enough, the synthetic images recovered from the ensemble approach (classifier + translation) achieve a better classification score than the original NBI sequences (0.86 vs 0.82, in F1-score). Such a fact may be associated with the dedication of drawn vascular patterns in enhanced synthetic images that may also act as a filter of light noise and associated artifacts in original sequences. There exists a gain of 4% in the F1-score and 10% in precision regarding the original NBI sequences, even considering that training was carried out over such original sequences.

Interestingly, the proposed approach (classifier ensemble) achieves competitive discrimination between polyp classes with scores that suggest strong support for expert opinion. Additional validation was carried out using embedding vectors (taken from \mathbf{f}_δ generator) as descriptors to discriminate grades of the disease and using a KNN rule for assign labels. In this sense, each of the colonoscopy frames is grouped in a cluster related to the particular video. In this regard, we expect to achieve a simple neoplastic prediction through the surrounding areas analysis by

Table 1. Classification performance over different colonoscopy sequences. From top to bottom rows, the classification criteria for the groups of expert and beginner gastroenterologists, real raw OC and NBI sequences, the only translation performance and classifier ensemble from synthetic images, and \mathbf{f}_δ embedding descriptors.

	Accuracy	Precision	Recall	F1-score
Gastroenterologist				
Experts	0.75	0.86	0.75	0.80
Beginners	0.83	0.80	1.00	0.89
Raw sequences				
OC	0.48	0.92	0.40	0.56
NBI	0.74	0.82	0.83	0.82
From synthetic images				
Only translation	0.70	0.90	0.72	0.80
Classifier ensemble	0.79	0.92	0.81	0.86
From embedding descriptors				
Only translation	0.63	0.94	0.59	0.72
Classifier ensemble	0.65	0.89	0.66	0.76

the KNN algorithm. It should be noticed that the classifier ensemble outperforms the baseline prediction by 4% in the F1-score metric. Despite this, the embedding vector’s performance is still limited and its use as a potential CRC descriptor remains a challenging task to be improved.

Table 2 shows detailed results for the expert’s and beginner’s medical criteria for all considered inputs. Interestingly, the hyperplastic samples are better discriminated by OC sequences than the NBI sequences, a fact associated with the not marked vascular patterns. From this class, the classification from embedding descriptors, trained only from a translation task, achieves also a perfect score in terms of complete video samples. It should be noted that for correct discrimination of adenomas, the discrimination should be carried out from NBI sequences. In such a line, the proposed approach (from synthetic images and embedding descriptors) achieves an enriched vascular representation of raw OC sequences, allowing better discrimination of adenomas. The ensemble approach forced to learn class distributions has better scores, achieving

86% for classification from synthetic images and 76% from embedding descriptors in the F1-score metric. In such case, this ensemble representation has an average gain of 6% regarding the approach that uses only translation, and an average gain of 30% regarding the OC sequences.

Table 2. Confusion matrix for adenoma-hyperplastic polyp classification in a video and frames (numbers inside the brackets) performance. From left to right, the group of experts and beginners' medical opinions, the classification performance over raw OC sequences, the real NBI sequences, the only translation task behavior, and finally, the classifier ensemble method. Interestingly, the classifier ensemble method (end-to-end scheme) outperforms the polyp pathology prediction.

		Only translation				Classifier ensemble								
Experts	Begginner	Xoc		nbi		\hat{x}_{nbi}		f_{δ} embedding		\hat{x}_{nbi}		f_{δ} embedding		
Ade	Hyp	Ade	Hyp	Ade	Hyp	Ade	Hyp	Ade	Hyp	Ade	Hyp	Ade	Hyp	
Ade	6 2	8 0	2 (1822) 6 (2702)	7 (3459) 1 (702)	5 (3247) 3 (1277)	6 (2648) 2 (1876)	6 (3683) 2 (841)	6 (2978) 2 (1546)						
Hyp	1 3	2 2	0 (162) 4 (790)	2 (764) 2 (613)	1 (356) 3 (596)	0 (160) 4 (792)	1 (327) 3 (625)	1 (377) 3 (575)						

Complementary, as an observational analysis, figure 7 is shown some polyp examples from different image modalities and enhancement alternatives, validating the three classes included in this study. In this figure, the columns correspond to different polyp samples; the respective rows are the OC frames, the respective synthetic responses, and the NBI frames. The highlighted red dotted boxes show examples with insufficient NBI pattern projection, as expected in the observed NBI sequences.

Remarkably, the synthetic approach using an ensemble classifier achieves more coherent synthetic observations, recovering both: vascular patterns but also textural color patterns around polyp masses. For instance, for the third polyp adenoma example, the intestinal fold is properly recovered without any artifacts (see mistakes in the bounding box for the strategy with only translation). It should be noted, that for the last serrated subplot, the proposed approach did not see examples during training and achieves a coherent reconstruction and mapping of NBI patterns over standard OC sequences. As expected, in such a case the classifier ensemble (bet-

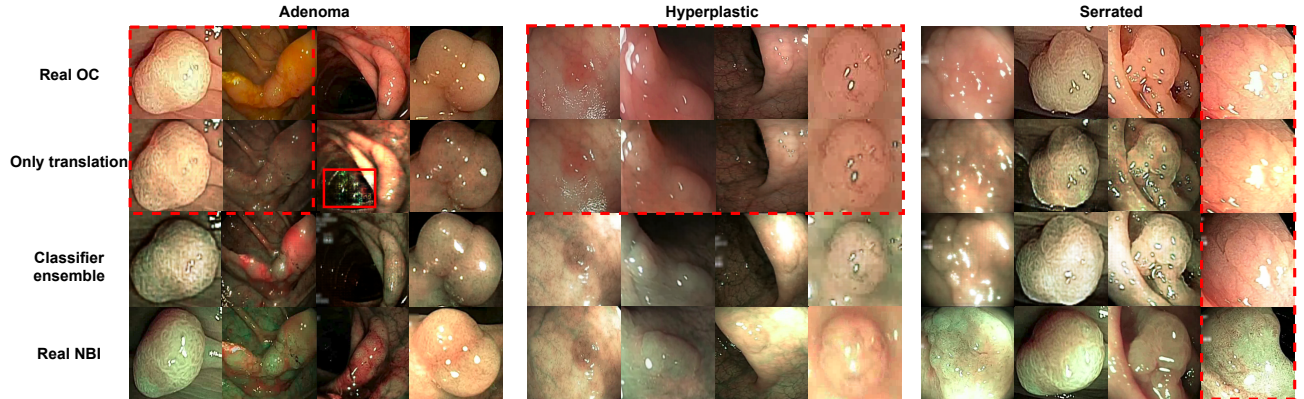


Figure 7. Enhanced adenoma and hyperplastic polyps OC images from NBI patterns. From top to bottom: colonoscopy representations for real OC, the only translation strategy and further classification, the classifier ensemble, and real NBI sequences. Dotted red lines reflect reconstructions far from the NBI expected representation. Interestingly the lacking of the neoplastic classifier network seems to affect the image generation by adding noise or even keeping the same OC representation. Serrated samples (used as an additional test set) reflect coherent vascular representations.

ween adenoma and hyperplastic) was not crucial for recovering synthetic images. In general, the proposed approach evidences outstanding results which may be potential as a clinical tool for vascular enhancement from typical OC sequences, and to carry out *in situ* procedures.

Serrated samples discrimination. A current challenge today in the diagnosis of colorectal cancer is the *in situ* discrimination of serrated samples (polyps with hyperplastic and adenoma visual patterns⁵). Hence, a key contribution of computational support should be addressed in the line of support such as serrated classification. Consequently, an extra study was conducted herein to validate the capability for discriminating serrated samples from raw output probabilities of the introduced translation approach, from synthetic images using only translation and ensemble architectures. Then, frames of three classes (including serrated) were mapped to the architectures, and then it recovered each respective adenoma probability.

Figure 8 shows the resultant distributions, discriminated for each projected class. In such a case, there is a notable difference, especially for probability populations that come from the

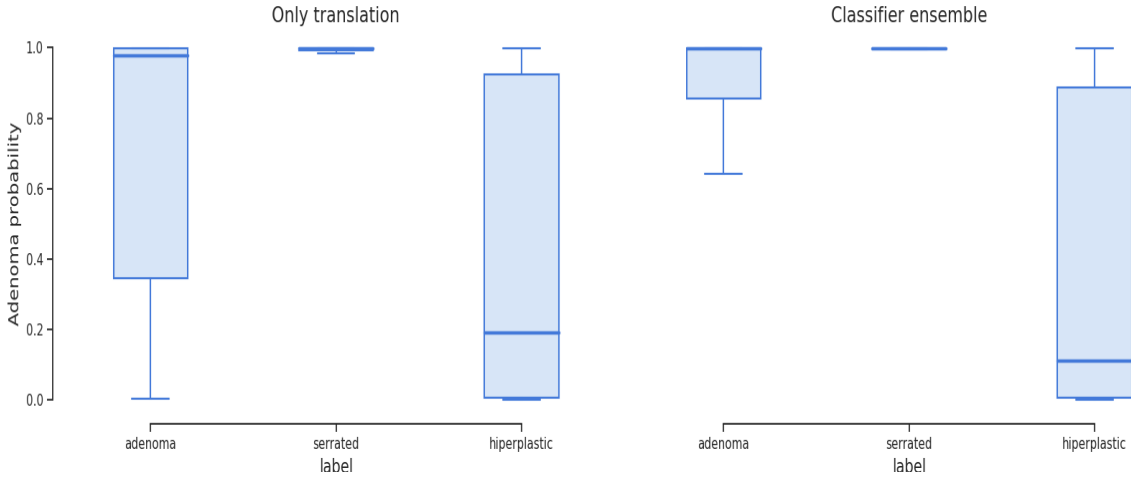


Figure 8. Boxplots for the related adenoma probability distributions using the three main kinds of polyps. From left to right the classification performance as an isolated task and the classifier ensemble scheme, respectively.

architecture with classifier ensemble. For the adenoma and hyperplastic samples, the associated neoplastic probability are fully apart each one outperforming the mean prediction by 10% for the adenoma biomarkers and lowering the neoplastic prediction in the hyperplastic samples by 3% regarding the only translation approach. Interestingly enough, the presented schemes achieve significative discrimination of serrated samples, even, when the architectures don't use such labels during training. As expected, the output probabilities from the ensemble architecture learn a major discriminative space, forcing to learn class distributions, and impacting also in a major discrimination of serrated samples. From a statistical test, we find significative differences ($p\text{-value} < 0.05$) according to the Mann-Whitney test.

Image translation. In this work also validated the quality of the reconstruction of synthetic images. For doing so, we take advantage of the explored subset with relatively paired adenoma and hyperplastic OC-NBI colonoscopy sequences ³³. This subset was analyzed from retrieved reconstruction, as well as, by the quality measures. A main challenge with such analysis is that a visual alignment among both observations (OC and NBI) is not always possible. For instance,

figure 9 shows some samples of the subset for adenoma and hyperplastic polyps.

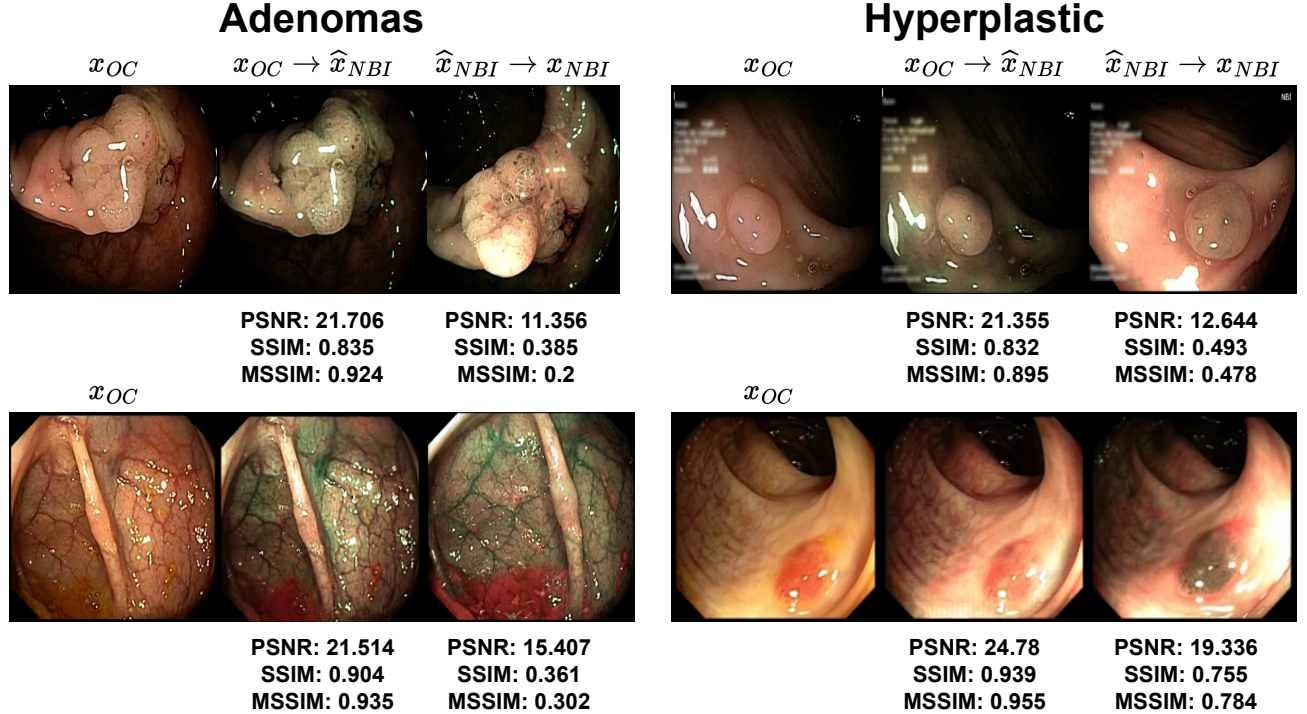


Figure 9. Image traduction quality over specific samples. The top row shows the quality performance over un-aligned samples while the bottom row for some visually aligned samples.

Despite the effort to achieve aligned samples, the top row evidences some unaligned samples, whose quantitative metrics are of course low due to the non-structural similarity between the images. To measure translation, it should be noted that reference and target images correspond to different domains. For instance, the maximum metrics values were achieved in the $x_{OC} \rightarrow \hat{x}_{NBI}$ representation, where $SSIM$ and $MSSIM$ are close to 90% and the $PSNR$ to 22. In such a case, the reported results should correspond to the gain in vascularity patterns, while the local structure is unchanged because the target comes from the same image reference. Contrary, the translation between $\hat{x}_{NBI} \rightarrow x_{nbi}$ (first row) abruptly changes the quantitative results, since polyp observation for reference is different w.r.t to the target in OC. Despite such changes, the metric report the adoption of some textural NBI patterns. The second row, it is showed some paired sequences with major alignment and the consequent impact on quantitative metrics.

To summarize, the quantitative metrics related to the reconstruction of relatively paired sequences, table 3 shows the average performance measured over such a public dataset. In this case, we validated the reconstruction achieved by the classifier ensemble, as well as, for the version that uses only translation. To do a major analysis, this subset was projected as a new test to the trained architectures, achieving an F1-score metric of 90, 2%, 93, 2%, and 95, 1% for the OC, $X_{OC} \rightarrow X_{NBI}$, and NBI sources, respectively.

Table 3. Image traduction quality over an aligned public dataset. Each column shows the performance from the original sample (left) to the desired target domain (right).

Metric	$X_{OC} \rightarrow$ Classifier ensemble	Only translation \rightarrow nbi	Classifier ensemble \rightarrow nbi
PSNR	22,973±1,465	15,226±2,748	15,226±2,748
SSIM	0,888±0,031	0,541±0,116	0,541±0,116
MSSIM	0,932±0,018	0,505±0,163	0,505±0,163

An extra validation was carried out from four collected colonoscopies, that include polyps diagnosed as adenomas. These videos were projected to the trained architecture and only used for test purposes. The whole projected frame achieved a correct score prediction, providing initial evidence about the generalization capability of the proposed strategy. Figure 10 shows the proposed approach performance enhancing the OC sequences. Interestingly, vascular patterns are coherently mapped.

Real OC



Classifier ensemble



Real NBI



Figure 10. Image traduction performance over owner dataset. Each column shows the OC enhancement performance over three different sequences. From top to bottom: the real OC sequences, the corresponding enhanced sequences, and real NBI representations, respectively.

7. DISCUSSION

In this study was introduced a translation task methodology was to enhance optical colonoscopy sequences, drawing vascular NBI patterns, allowing a better approximation for polyp malignancy discrimination. For doing so, a deep representation was adjusted from a translation ($OC \rightarrow NBI$) task, following a non-aligned perspective. The proposed approach demonstrated that enriched synthetic frames achieved a classification gain of around 30% in the F1-score metric, regarding standard colonoscopies. Besides, the proposed approach included a malignancy discrimination branch, which forces generative distributions to classify polyps according to the malignancy. The capability of computational approaches was compared to gastroenterologist beginners and experts. According to validation, the proposed approach outperformed expert opinion by around 6% in the F1-score metric, when such experts observed the NBI original sequences. Such a fact may be associated with more complex synthetic sequences focusing on vascular polyp patterns and filtering out additional image artifacts that may confuse expert observations. The reported results evidenced potential capabilities of translation approaches to be implemented in clinical routine and achieve *in situ* polyp classification, avoiding limitations associated with precise sample recovering, and time of analysis, among others. Interestingly enough, the proposed approach can correlate the serrated samples (the main challenge through the clinical routine) with the neoplasia degree, establishing a statistical difference from adenoma, hyperplastic and serrated samples with a p-value < 0.05 according to the Mann-Whitney test.

From standard optical colonoscopies, some computational approaches have approximated the problem of polyp classification. For instance, geometric, color, and textural features have been combined to approximate polyp malignancy (in a dataset with 76 videos samples obtained an accuracy = 87% with random forest ²⁶ and 74% from a combination of features and a Random Subspaces classifier ¹⁵). Other approaches have used convolutional deep features to model polyp

classes, achieving 67.3 % of accuracy in a dataset with 3828 samples³⁰. These approaches are limited by optical observations and many times require preprocessing and exclusion of blurring frames. More recent approaches have integrated, OC, NBI, and sequences with contrast to discriminate polyps, reporting an average of 90% (validation from 180 frames by each source), evidencing the classification improvement by using complementary observations²⁵. Also, high-definition NBI sequences have been complemented with blue laser images (BLI) to achieve a more sensible classification under *SANO* protocol, achieving an AUC of 94.3% and 84.5% for internal and external datasets with 1235 and 69 samples, respectively¹. These methods, nonetheless, require clear and magnified polyp screenshots. Contrary, the proposed approach, adjusted from a pretext task, has major robustness to code malignancy according to vascular observations and includes high variability in the sequences. Besides, the proposed scheme is realistic to transfer in clinical scenarios without dependency on special tools, agents, or complementary sequences to carry out the analysis. In such a case, the proposed approach achieved a remarked 81% recall from synthetic images, recovering 9/12 total test video sequences. Also, taking embedding low-dimensional descriptors, it was possible to have a coherent rate of discrimination, achieving an F1-average score of 76%. These results were captured in whole sequences without exclusion criteria about recording conditions (poor light conditions, strong camera movements, among others).

Also, the literature has proposed a teacher-student architecture for translation tasks but using an alignment approximation between optical and NBI sequences³³. This work achieved a mean accuracy of 85.3% in a controlled experiment with only 307 and 116 frames for the adenoma and hyperplastic samples, respectively. Similarly, Ma *et al.* proposes a translation of paired training for an attention architecture, learning an embedding space with a polyp class discrimination capability with an average accuracy of 87.7%³⁴. Regarding such methodology, the proposed approach operates into a non-aligned scheme, allowing more flexibility to learn polyp class distribution with advantages even in training (major samples to adjust the representation, 5632

frames in our case). This unpaired criterion is closer to application *i.e.*, there are no OC and NBI sequences, projected at the same time.

During the validation, the adjusted deep representation was validated concerning the capability to discriminate serrated samples. Remarkably, the output probabilities demonstrated a capability to also discriminate serrated samples, with statistical test confidence (Mann-Whitney test $\rho < 0.05$). Such a point result is particularly interesting since serrated samples represent a major challenge today in clinical routine, and maybe a key issue to define the malignancy of an observed polyp. Hence, the proposed approach can discriminate between adenoma and hyperplastic samples, but also, this approach has sufficient sensibility to separate as a neoplastic lesion in the 93.4% of the serrated samples. The discrimination of three classes was achieved from synthetic enhanced images but also from the resultant embedding representation. Future perspectives may be addressed to robustly model label information about samples and the operation in more realistic scenarios, where the switch from OC to NBI can be perceived by the approach. Also, future works include the study and modeling of complementary generative mechanisms to lead to high and uncontrolled variability of colonoscopy sequences.

8. CONCLUSIONS AND FUTURE WORK

This work presented a methodology to compute enhanced optical colonoscopy that aggregates vascular patterns from NBI observations. For doing so, a deep translation architecture was proposed to enhance optical images, which in turn have a major discrimination capability between adenoma and hyperplastic samples. In the translation, representation adopted a malignancy classification network that allows a better image synthesis with also coherent discrimination among classes. The proposed approach achieved competitive results and the achieved synthetic images suggest a potential capability to be used in clinical scenarios.

Future works and perspectives include the exploration and proposal of a new generative representation that outperforms the current optical enhancement and better recovers vascular NBI patterns. Also, the exploration of the attention mechanism can be useful to retrieve the best components that impact in discrimination of polyp malignancy. Finally, these approaches should be validated in larger datasets with long colonoscopy observations to lead to the generalization of proposed tools.

BIBLIOGRAPHY

- Bora, Kangkana et al. “Computational learning of features for automated colonic polyp classification”. In: *Scientific Reports* 11.1 (2021), pp. 1–16 (cit. on p. 11).
- Chen, Jiawei et al. “Generative adversarial networks for video-to-video domain adaptation”. In: *Proceedings of the AAAI Conference on Artificial Intelligence*. Vol. 34. 04. 2020, pp. 3462–3469 (cit. on p. 13).
- Chen, Peng-Jen et al. “Accurate classification of diminutive colorectal polyps using computer-aided analysis”. In: *Gastroenterology* 154.3 (2018), pp. 568–575 (cit. on p. 22).
- Cincar, Kristijan and Ioan Sima. “Machine Learning algorithms approach for Gastrointestinal Polyps classification”. In: *2020 International Conference on INnovations in Intelligent SysTems and Applications (INISTA)*. IEEE. 2020, pp. 1–6 (cit. on pp. 22, 46).
- Cocomazzi, Francesco et al. “Accuracy and inter-observer agreement of the nice and kudo classifications of superficial colonic lesions: a comparative study”. In: *International journal of colorectal disease* (2021), pp. 1–8 (cit. on pp. 12, 15, 24).
- Cohen, Joseph Paul, Margaux Luck, and Sina Honari. “Distribution matching losses can hallucinate features in medical image translation”. In: *Medical Image Computing and Computer Assisted Intervention–MICCAI 2018: 21st International Conference, Granada, Spain, September 16–20, 2018, Proceedings, Part I*. Springer. 2018, pp. 529–536 (cit. on p. 20).
- Fukuda, Akihiro et al. “Generating virtual chromoendoscopic images and improving detectability and classification performance of endoscopic lesions”. In: *Domain Adaptation and Represen-*

tation Transfer and Medical Image Learning with Less Labels and Imperfect Data. Springer, 2019, pp. 99–107 (cit. on p. 13).

Gross, Sebastian et al. “Computer-based classification of small colorectal polyps by using narrow-band imaging with optical magnification”. In: *Gastrointestinal endoscopy* 74.6 (2011), pp. 1354–1359 (cit. on p. 22).

Haumaier, Franziska, William Sterlacci, and Michael Vieth. “Histological and molecular classification of gastrointestinal polyps”. In: *Best Practice & Research Clinical Gastroenterology* 31.4 (2017), pp. 369–379 (cit. on pp. 16, 24, 33).

Horiuchi, Yusuke et al. “Convolutional neural network for differentiating gastric cancer from gastritis using magnified endoscopy with narrow band imaging”. In: *Digestive diseases and sciences* 65 (2020), pp. 1355–1363 (cit. on p. 22).

Isola, Phillip et al. “Image-to-image translation with conditional adversarial networks”. In: *Proceedings of the IEEE conference on computer vision and pattern recognition*. 2017, pp. 1125–1134 (cit. on p. 35).

Kaltenbach, Tonya et al. “Endoscopic removal of colorectal lesions—recommendations by the US Multi-Society Task Force on Colorectal Cancer”. In: *Gastroenterology* 158.4 (2020), pp. 1095–1129 (cit. on p. 12).

Kim, David H et al. “Serrated polyps at CT colonography: prevalence and characteristics of the serrated polyp spectrum”. In: *Radiology* 280.2 (2016), pp. 455–463 (cit. on pp. 17, 24).

Li, Lan et al. “Convolutional neural network for the diagnosis of early gastric cancer based on magnifying narrow band imaging”. In: *Gastric Cancer* 23 (2020), pp. 126–132 (cit. on p. 22).

Longacre, Teri A and Cecilia M Fenoglio-Preiser. “Mixed hyperplastic adenomatous polyps/serrated adenomas. A distinct form of colorectal neoplasia.” In: *The American journal of surgical pathology* 14.6 (1990), pp. 524–537 (cit. on pp. 14, 16, 17, 24).

Ma, Weijie et al. “Toward Clinically Assisted Colorectal Polyp Recognition via Structured Cross-Modal Representation Consistency”. In: *International Conference on Medical Image Computing and Computer-Assisted Intervention*. Springer. 2022, pp. 141–150 (cit. on pp. 23, 25, 47).

Mesejo, Pablo et al. “Computer-aided classification of gastrointestinal lesions in regular colonoscopy”. In: *IEEE transactions on medical imaging* 35.9 (2016), pp. 2051–2063 (cit. on pp. 15, 46).

Mori, Yuichi et al. “Computer-aided diagnosis for colonoscopy”. In: *Endoscopy* 49.08 (2017), pp. 813–819 (cit. on p. 19).

Moussata, Driffa et al. “Endoscopic and histologic characteristics of serrated lesions”. In: *World journal of gastroenterology: WJG* 21.10 (2015), p. 2896 (cit. on p. 12).

Okamoto, Koichi et al. “Clinicopathological characteristics of serrated polyps as precursors to colorectal cancer: current status and management”. In: *Journal of gastroenterology and hepatology* 32.2 (2017), pp. 358–367 (cit. on pp. 12, 17, 22).

Ortega-Morán, Juan Francisco et al. “Medical needs related to the endoscopic technology and colonoscopy for colorectal cancer diagnosis”. In: *BMC cancer* 21.1 (2021), pp. 1–12 (cit. on pp. 11–13, 15–17, 19, 23).

Ozawa, Tsuyoshi et al. “Automated endoscopic detection and classification of colorectal polyps using convolutional neural networks”. In: *Therapeutic advances in gastroenterology* 13 (2020), p. 1756284820910659 (cit. on p. 23).

Pu, Leonardo Zorron Cheng Tao et al. “Computer-aided diagnosis for characterization of colorectal lesions: comprehensive software that includes differentiation of serrated lesions”. In: *Gastrointestinal endoscopy* 92.4 (2020), pp. 891–899 (cit. on pp. 11, 47).

Puig, Ignasi and Tonya Kaltenbach. “Optical diagnosis for colorectal polyps: a useful technique now or in the future?” In: *Gut and Liver* 12.4 (2018), p. 385 (cit. on pp. 11, 15, 24, 41).

Rawla, Prashanth, Tagore Sunkara, and Adam Barsouk. “Epidemiology of colorectal cancer: incidence, mortality, survival, and risk factors”. In: *Przeglad gastroenterologiczny* 14.2 (2019), p. 89 (cit. on pp. 11, 14, 24).

Rodriguez-Diaz, Eladio et al. “Real-time artificial intelligence-based histologic classification of colorectal polyps with augmented visualization”. In: *Gastrointestinal Endoscopy* 93.3 (2021), pp. 662–670 (cit. on p. 23).

Sánchez-Montes, Cristina et al. “Computer-aided prediction of polyp histology on white light colonoscopy using surface pattern analysis”. In: *Endoscopy* 51.03 (2019), pp. 261–265 (cit. on p. 25).

Sierra-Jerez, Franklin, Jair Ruiz, and Fabio Martínez. “A Non-Aligned Deep Representation to Enhance Standard Colonoscopy Observations from Vascular Narrow Band Polyp Patterns.” In: *2022 44th Annual International Conference of the IEEE Engineering in Medicine & Biology Society (EMBC)*. IEEE. 2022, pp. 1671–1674 (cit. on p. 27).

Song, Eun Mi et al. “Endoscopic diagnosis and treatment planning for colorectal polyps using a deep-learning model”. In: *Scientific reports* 10.1 (2020), pp. 1–10 (cit. on p. 24).

Sung, Hyuna et al. “Global cancer statistics 2020: GLOBOCAN estimates of incidence and mortality worldwide for 36 cancers in 185 countries”. In: *CA: a cancer journal for clinicians* 71.3 (2021), pp. 209–249 (cit. on pp. 11, 24).

Ueyama, Hiroya et al. “Application of artificial intelligence using a convolutional neural network for diagnosis of early gastric cancer based on magnifying endoscopy with narrow-band imaging”. In: *Journal of gastroenterology and hepatology* 36.2 (2021), pp. 482–489 (cit. on p. 22).

Urban, Gregor et al. “Deep learning localizes and identifies polyps in real time with 96% accuracy in screening colonoscopy”. In: *Gastroenterology* 155.4 (2018), pp. 1069–1078 (cit. on p. 16).

Usami, Hiroyasu et al. “Colorectal polyp classification based on latent sharing features domain from multiple endoscopy images”. In: *Procedia Computer Science* 176 (2020), pp. 2507–2514 (cit. on pp. 22, 47).

Vişovan, Irina Ioana et al. “The role of narrow band imaging in colorectal polyp detection”. In: *Bosnian journal of basic medical sciences* 17.2 (2017), p. 152 (cit. on pp. 12, 24).

Wang, Qin et al. “Colorectal Polyp Classification from White-Light Colonoscopy Images via Domain Alignment”. In: *International Conference on Medical Image Computing and Computer-Assisted Intervention*. Springer. 2021, pp. 24–32 (cit. on pp. 23, 25, 32, 42, 47).

Yang, Young Joo et al. “Automated classification of colorectal neoplasms in white-light colonoscopy images via deep learning”. In: *Journal of clinical medicine* 9.5 (2020), p. 1593 (cit. on pp. 23, 47).

Zhang, Ruikai et al. “Automatic detection and classification of colorectal polyps by transferring low-level CNN features from nonmedical domain”. In: *IEEE journal of biomedical and health informatics* 21.1 (2016), pp. 41–47 (cit. on pp. 16, 33).

Zhu, Jun-Yan et al. “Unpaired image-to-image translation using cycle-consistent adversarial networks”. In: *Proceedings of the IEEE international conference on computer vision*. 2017, pp. 2223–2232 (cit. on pp. 19, 28).

APPENDIX OF ACADEMIC PRODUCTS

Anexo A. Academic Products

Journals

- F. Sierra-Jerez, F. Martínez "Polyp malignancy classification from a non-aligned translation between optical and NBI colonoscopies". Biomedical Informatics
Status: Submitted
- L. Ruiz, F. Sierra-Jerez, F. Martínez "Polyp segmentation and classification from multi-tasks cross-attention strategy". Journal of Medical Imaging. 2023.
Status: Submitted

Conference papers:

F. Sierra-Jerez, J. Ruiz, F. Martínez. "A Non-Aligned Deep Representation to Enhance Standard Colonoscopy Observations from Vascular Narrow Band Polyp Patterns". 44th Annual International Conference of the IEEE Engineering in Medicine & Biology Society (EMBC). 2022.

Status: Published.